Contract No:

This document was prepared in conjunction with work accomplished under Contract No. DE-AC09-08SR22470 with the U.S. Department of Energy (DOE) Office of Environmental Management (EM).

Disclaimer:

Evolution of Corrosion Potential of Carbon Steel Storage Tanks Containing High-Level Nuclear Waste

Pavan K. Shukla, Roderick E. Fuentes, and Bruce J. Wiersma
Savannah River National Laboratory®
Aiken, South Carolina, 29808
USA

and

Crystal Girardot and Jason Page
Washington River Protection Solutions
2425 Stevens Center Pl
Richland, Washington, 99352
USA

ABSTRACT

Millions of gallons of high-level radioactive waste are stored in underground carbon-steel storage tanks at the Hanford site. The waste chemistries are mixtures of organic and inorganic species and are predominantly alkaline. Tank corrosion conditions are partly monitored by measuring corrosion potentials of the tank carbon-steel. In addition, independent studies are conducted using chemical simulants representing the tank waste chemistries. It has been observed that several tanks' corrosion potentials are invariant with time, however, laboratory experiment data with the simulants exhibit time-dependent evolutions of the corrosion potentials for several tank waste chemistries. Laboratory experimental data is used to assess the risk of pitting and stress corrosion cracking of the tank walls, and corrosion potential is one of the important parameters in the risk assessment matrix. Therefore, it is important to understand source of corrosion potential evolutions and their implications on the risk assessment. To this end, laboratory experiments were conducted with the simulants of three tank chemistries. Corrosion potential evolutions were measured. The tank steel conditions were represented in each simulant using three coupons with following surfaces: (i) polished, (ii) mill-scale with corrosion products, and (iii) partly polished surface of a mill-scale coupon. The electrochemical experiments were conducted for approximately 4 months, and corrosion potential evolutions were recorded. This paper presents the electrochemical test results and provides quantification of the evolutions as a function of surface characteristics and waste chemistries. The paper also explores sources of corrosion potential evolutions observed in the experiments.

Key words: Open-circuit potential, passive film, Hanford, high-level radioactive waste

INTRODUCTION

The Hanford site in Washington state has 177 carbon steel tanks storing approximately 208 million liters of radioactive waste. Long-term structural integrity of the tanks is dependent on maintaining the waste chemistry that does not promote pitting and stress corrosion cracking. Corrosion potential, i.e., OCP, is an indicator of pitting

corrosion tendency for a material in contact with an environment. Specifically, if the corrosion potential is greater than the repassivation potential, pitting corrosion could initiate and propagate. The repassivation potential provides a measure of a materials corrosion related properties under anoxic conditions.[1] The corrosion potential, on the other hand, is a measure of chemical kinetic equilibrium between anodic and cathodic reactions. If the corrosion potential changes with time, especially if it shifts in the anodic direction, this may be an indication of an increase in pitting corrosion susceptibility of the material exposed to a given environment. Chawla et al.[2] and Evans et al.[3] conjectured that anodic drift in the corrosion potential could be due to the change in electronic properties of the passive films. They concluded that anodic drift cannot be explained by electrochemical testing alone, and additional studies on anodic and cathodic reaction kinetics are needed to understand and explain the anodic drift.

Cyclic potentiodynamic polarization (CPP) experiments are conducted to identify risk of pitting corrosion, and subsequently determine the level of inhibition needed to mitigate the pitting corrosion. CPP experimental steps are derived from ASTM G61, and the current versus potential measurements are started two hours after an experiment has been setup.[4] The derived procedure is slightly different from the one detailed in ASTM G61.[5,6] CPP data are generally used to measure tendency of repassivation including repassivation potential, and it is assumed that corrosion potential is steady during the measurement and thereafter. In addition, it is implicitly assumed that the corrosion potential measured at the start of a CPP measurement is sufficient for the pitting corrosion risk analysis.

One key difference between laboratory testing using CPP and field conditions has been coupon surface condition used in the laboratory testing in comparison to the tanks' construction material condition. CPP tests have been conducted using the 600-grit-polished bullet coupons [6,5] whereas the tank steel has naturally occurring mill-scale plus corrosion products on the surface. It is recognized that during the construction process, large sheets of the carbon-steel metal were welded together, and other processes associated with tank construction could have disturbed the original mill-scale on the coupons. Considering this, a 600-grit polished coupon was utilized as one extreme of the surface condition whereas a coupon with mill-scale plus corrosion products is considered the other extreme. The surface condition of a newly constructed tank is expected to be somewhere between the two extremes. In addition, the tanks were commissioned sometime after completion of construction. This would have provided the tank steel to be exposed to ambient conditions and develop additional layers or corrosion products before in-service placement. Considering several possibilities of the surface conditions, the objective of the study also included determining effect of surface condition on evolution of OCP.

This study was focused on determining extent and source of potential drift/no drift in the operating tanks at Hanford. Laboratory experiments were conducted to determine the extent and source of the drift. Specifically, the corrosion potential drift data were measured along with the corrosion current density and polarization resistance data. Three simulant chemistries were selected. Coupons with varying surface conditions were placed in the chemistries. Open circuit potentials of the coupons were monitored over a period of four months. Following this, electrochemical impedance spectroscopy (EIS) and CPP measurements of the coupons were conducted in sequence. The OCP, EIS, and CPP data were analyzed to determine the extent and source of the potential drifts.

EXPERIMENTAL

Several corrosion cells were setup with multiple electrodes, with each corrosion cell containing at most three working electrodes. The working electrodes were fabricated from Association of American Railroads[(1)] Tank Car (AAR TC 128) steel since it approximates the chemistry and microstructure of the vintage steel from which the tanks were fabricated, UNS K02401 (i.e., American Society for Testing and Materials (ASTM) [(2)] A515 Grade 60 carbon steel). Table 1 lists the chemical composition for the steel. All elemental compositions except for Mn and Si meet the ASTM specification. The coupons are categorized in three different sets for their surface characteristics. The first set of three coupons included 600-grit polished bullets, routinely used in the CPP tests. An image of the one of the bullet coupons is presented in Figure 1(a). The second set of the three coupons were cut outs from a rail-road car steel piece with mill-scale plus corrosion product on one face of each coupon. The second set coupons were mounted in epoxy with the exposed surface being the one with mill-scale plus corrosion products. An image of the coupons in the second set is presented in Figure 1(b). The third set coupons were

[(1)] American Association of Railroads, 425 3rd Street SW, Washington, DC 20024
[(2)] ASTM International, 100 Barr Harbor Dr., West Conshohocken, PA 19428-2959

modified versions of the coupons with mill-scale plus corrosion products surfaces. In the third set, approximately one fourth of the coupon surface was machined to remove the mill-scale and corrosion products. An image of the coupons in the second set is presented in Figure 1(c). The coupons are identified as following hereafter: (i) bullet [Figure 1(a)], and (ii) mill-scale plus corrosion products [Figure 1(b)].

Table 1
Chemical Composition of AAR TC 128 Steel (wt.%)

	C	Mn	P	S	Si	Fe
Specification	0.24 (max.)	0.9 (max.)	0.035 (max.)	0.04 (max.)	0.13 to 0.33	Balance
Measured	0.212	1.029	0.012	0.013	0.061	Balance

(a) 600 grit polished surface bullet coupon (3.175-cm length × 0.478-cm diameter)

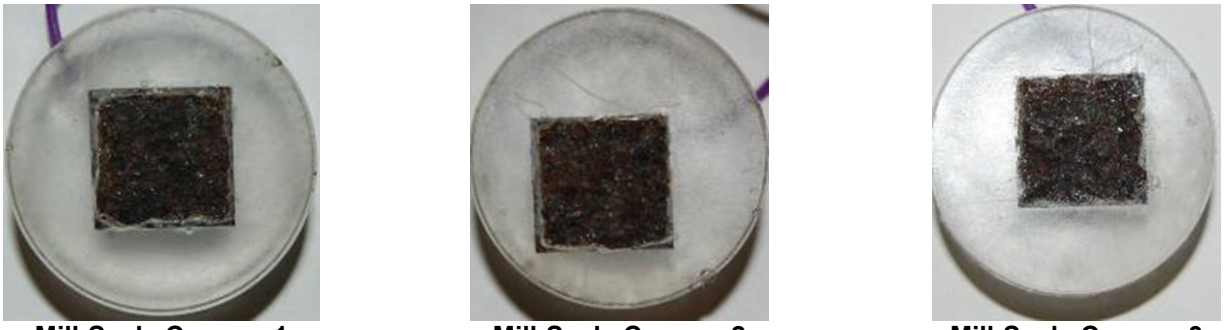

Mill-Scale Coupon 1 **Mill-Scale Coupon 2** **Mill-Scale Coupon 3**

(b) Three 1.5 cm × 1.5 cm × 1.0 cm coupons cut out of rail road car steel with mill-scale plus corrosion product on the exposed surface

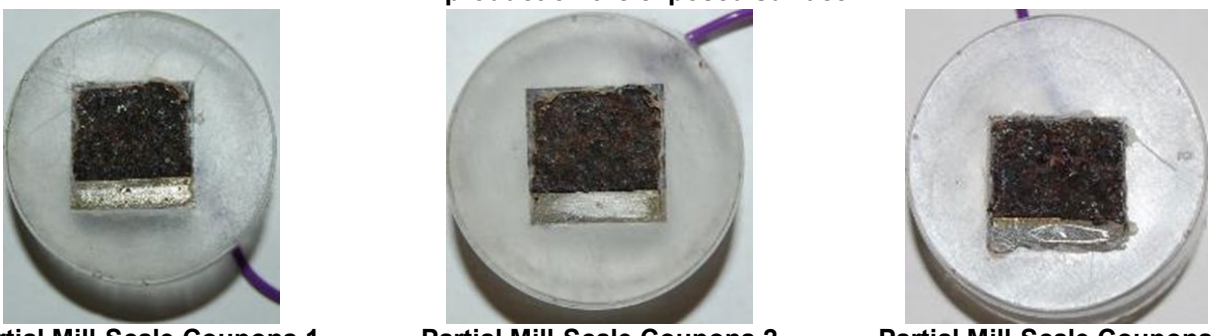

Partial Mill-Scale Coupons 1 **Partial Mill-Scale Coupons 2** **Partial Mill-Scale Coupons 3**

(c) Three 1.5 cm × 1.5 cm × 1.0 cm coupons cut out of rail road car steel with mill-scale plus corrosion product partly removed from the surface on the exposed side

Figure 1: Images of the coupons used to study evolution of open circuit potential as a function of surface condition in three different simulants

One of the key differences between the bullet and mill-scale three coupons was immediately observed during electrical resistance measurements. Two probes of a resistance meter were placed across thickness of the coupons, with one probe being on the exposed surface. Electrical resistance of the bullet coupon was nearly independent of the probe positions and was less than 0.1 Ω in all measurements. Electrical resistance of the mill-scale coupons varied with the position of the probe on the exposed surface, and resistance values range

varied for each mill-scale plus corrosion products coupon; the resistance values ranged between 194 Ω to 0.7 MΩ. The resistance data indicated that mill scale plus corrosion products provide an electronic barrier to charge flow compared to the bullet coupons, however, the resistance values are location dependent. Resistance of the partial mill-scale coupons also varied with the position of the probe. When probe was placed on the area where mill-scale layer was removed, the resistance values ranged between 0.1 to 0.6 Ω, however, when the probe was placed in the area covered with the mill-scale and corrosion product layer, the resistance values ranged between 467 Ω to 7.8 MΩ. This indicates that the parts (where mill-scale is removed) of the partial mill-scale coupons are akin to the bullet coupons whereas the parts of the coupon covered with the mill-scale and corrosion products is akin to the mill-scale coupons. Thus, the partial mill-scale coupons represent a surface condition in between the bullet and mill-scale coupons.

The experiments were conducted with three Hanford waste simulants as the electrolytes to study the OCP evolution. These simulants are identified as AY-101, AW-105, and SY-101. To study the effects of organics species in AW-105, three versions of the AW-105 were developed: (i) AW-105 with small organic acids such as formate, acetate, and glycolate, (ii) AW-105 with small organic acids plus tributylphosphate family organics plus normal paraffin hydrocarbons, and (iii) AW-105 with small organic acids plus spiked tributylphosphate family organics plus normal paraffin hydrocarbon. Chemical composition of the AY-101, AW-105 with small organics, and SY-101 are listed in Table 2. Chemical compositions of the AW-105 with small organic acids plus tributylphosphate family organics plus normal paraffin hydrocarbons are partially listed in Table 3; the remaining species in this simulant are same as in AW-105 with small organic acids. Similarly, chemical compositions of the AW-105 with small organic acids plus spiked tributylphosphate family organics plus normal paraffin hydrocarbons are partially listed in Table 3; the remaining species in this simulant are same as in AW-105 with small organic acids.

Table 2
Chemical Composition of the Simulants Used to Study Evolution of Open Circuit Potential

Chemical	Concentration (M)		
	AY-101	**AW-105 with small organic acids (i.e., formate, acetate, glycolate)**	**SY-101**
Sodium hydroxide	0.688	1.735	0.600
Sodium nitrite	1.251	1.000	0.259
Sodium nitrate	1.911	1.101	1.032
Sodium chloride	0.070	0.046	0.027
Sodium fluoride	0.025	0.108	0.021
Sodium sulfate	0.056	0.021	0.020
Trisodium phosphate, 12-hydrate	0.036	0.012	0.083
Sodium carbonate	0.743	0.751	0.206
Sodium bicarbonate	0.000		0.001
Sodium formate	0.026	0.008	0.010
Sodium acetate, 3-hydrate	0.012	0.012	0.003
Sodium glycolate	0.0029		0.003
Sodium oxalate	0.0062	0.004	0.022
Ammonium bicarbonate	0.0013	0.00866	0.006
Sodium aluminate	0.261	0.324	0.131
Potassium nitrate	0.089	0.719	0.008
Solution pH at 21 °C	14	14	14

Table 3
Chemical Composition of AW 105 with Higher Organics

Chemical	Concentration (M)	
	AW-105 with small organic acids, tributylphosphate family, normal paraffin hydrocarbon	AW-105 with small organic acids, spiked tributylphosphate family, normal paraffin hydrocarbon
Propionic acid	0.0000703	0.0000703
Sodium acetate, 3 hydrate	0.012	0.12
Sodium glycolate	0.0029	0.029
Sodium butyrate	0.000149	0.000149
Tributyl phosphate	0.0000412	0.0000412
1-Butanol	0.000177	0.000177
n-butyl phosphate: mixture of mono-n-butyl and di-n-butyl	0.0034	0.034
Bis(2-ethylhexyl)phtalate	2.80E-06	2.80E-06
2-methyl-2-nitrobutane (tert-nitrobutane)	0.000719	0.000719
tetradecanoate (myristic acid)	1.00E-05	1.00E-05
Butanone-2 (ethyl methyl ketone)	0.00001	0.00001
Methylbutanone-2 (3-hydroxy-3-methyl-2-butanone)	0.00001	0.00001
Undecane	1.00E-08	1.00E-08
Dodecane	1.00E-08	1.00E-08
Tridecane	1.00E-08	1.00E-08
Tetradecane	1.00E-08	1.00E-08
1-Octanol	1.00E-06	1.00E-06
2-Octanone	1.00E-06	1.00E-06
Octanoate (ethyl octanoate)	1.00E-05	1.00E-05
1-Tetradecanol (myristil alcohol)	1.00E-06	1.00E-06
2-Tetradecanone	1.00E-06	1.00E-06

All experiments were conducted at 35 °C, and atmospheric pressure. All potentials were measured with respect to saturated calomel reference electrode (SCE).

EXPERIMENTAL DATA AND RESULTS

The OCP data for the bullet and mill-scale and partial mill-scale coupons in the various simulants were collected for up to 5 months. The OCP data for the three coupons in AY-101 simulant are presented in Figure 2. Initial OCPs of the bullet, mill-scale, and partial mill-scale coupons are -557, -176, and -388 mV_{SCE}, respectively. The potentials of the three electrodes quickly evolved and eventually settled to approximately -140 mV_{SCE} for the bullet, mill-scale, and partial mill-scale coupons after four months of evolution; this indicates that terminal OCPs are independent of the surface finish in AY-101.

The OCP data for the three coupons in SY-101 simulant are presented in Figure 3. Initial OCPs of the bullet, mill-scale, and partial mill-scale coupons are -492, -183, and -323 mV_{SCE}, respectively. In the first 500 hours, the potentials of the three electrodes quickly evolved, however, the rate of evolution became slow thereafter. The OCPs of the electrode after 4000 hours are following: -74 mV_{SCE}, -298 mV_{SCE}, and -340 mV_{SCE} for the bullet,

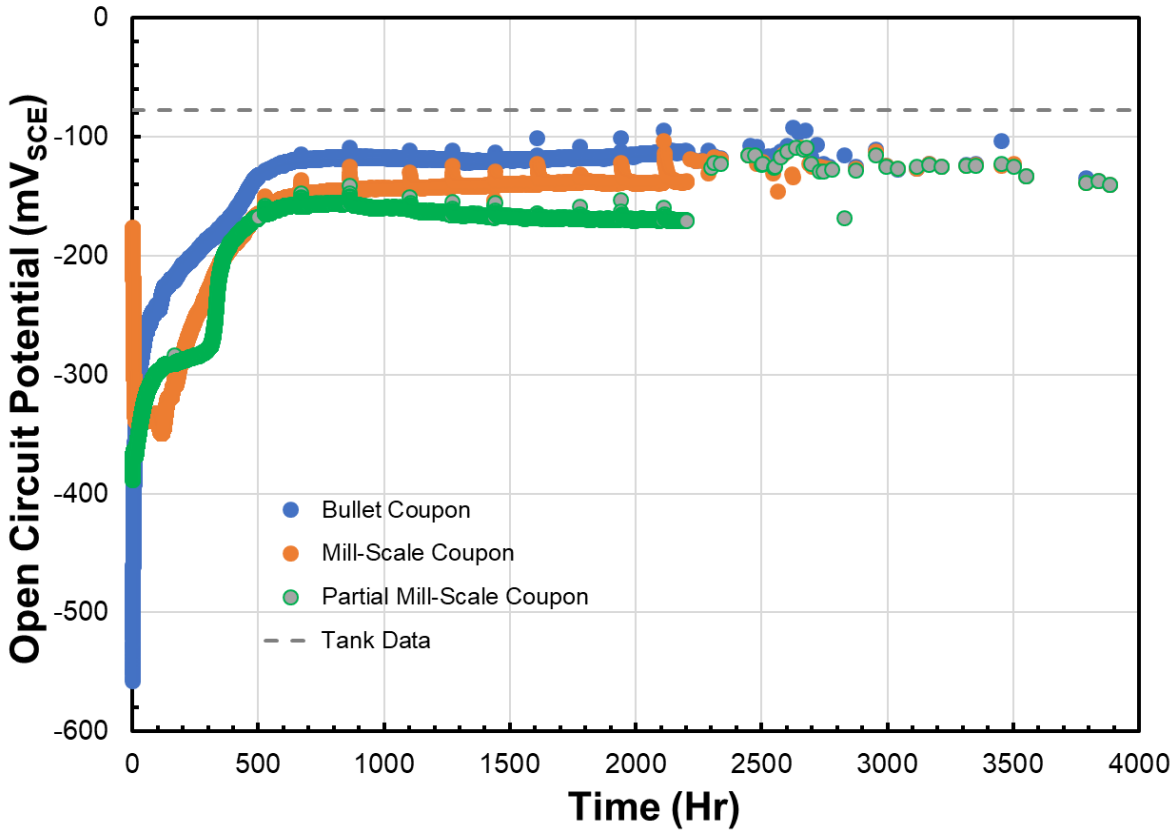

Figure 2: Open Circuit Potential data for the bullet (600-grit polished surface), mill-scale, and partial mill-scale coupons in AY-101 simulant

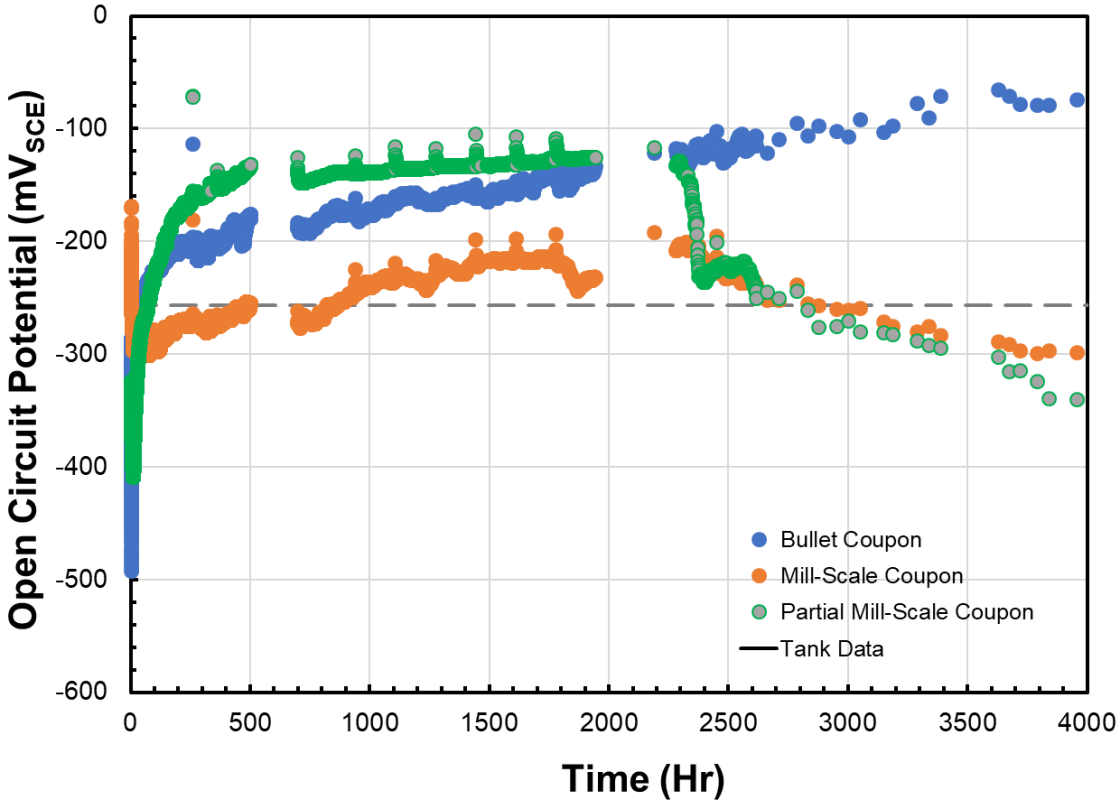

Figure 3: Open Circuit Potential data for the bullet (600-grit polished surface), mill-scale, and partial mill-scale coupons in SY-101 simulant

mill-scale, and partial mill-scale coupons. As seen in Figure 3, the potentials continued to evolve even after 4000 hours of exposure, and did not reach steady state. The potentials of the partial mill-scale coupon suddenly shifted to more-negative values after 2300 hours, as seen in Figure 3; this shift caused the potentials of the mill-scale and partial mill-scale coupons to be close to each other, and thus potentials of the two electrodes were at least 200 mV more cathodic than the polished surface, i.e., bullet coupon.

The OCP data for the three coupons in AW-105 simulant with small organic acids are presented in Figure 4. Initial OCPs of the bullet, mill-scale, and partial mill-scale coupons are -668, -284, and -405 mV_{SCE}, respectively. In the first 500 hours, the potentials of the three electrodes quickly evolved, however, the rate of evolution became slow thereafter. The OCPs of the electrode after 4000 hours are following: -256 mV_{SCE} , -186 mV_{SCE} , and -319 mV_{SCE} for the bullet, mill-scale, and partial mill-scale coupons.

The OCP data for the bullet and mill-scale coupons in AW-105 simulant with small organic acids plus tributylphosphate family plus normal paraffin hydrocarbons are presented in Figure 5. Initial OCPs of the bullet and mill-scale coupons are -516 and -205 mV_{SCE}, respectively. In the first 10 hours, the potentials of the two coupons quickly evolved. The OCPs of the electrode after 1200 hours are following: -239 mV_{SCE} and -251 mV_{SCE} for the bullet and mill-scale coupons, respectively.

The OCP data for the three coupons in AW-105 simulant with small organic acids plus spiked tributylphosphate family plus normal paraffin hydrocarbons are presented in Figure 6. Initial OCPs of the bullet, mill-scale, and partial mill-scale coupons are -893, -300, and -299 mV_{SCE}, respectively. In the first 100 hours, the potentials of the three electrodes quickly evolved, however, the rate of evolution became slow thereafter. The OCPs of the coupons after 2350 hours are following: -494 mV_{SCE} , -459 mV_{SCE} , and -480 mV_{SCE} for the bullet, mill-scale, and partial mill-scale coupons. The initial and the last OCPs are listed in Table 4. Figures 2-6 also contain the actual tank data which are represented by gray dash line in each figure. The actual tank data are listed in Table 5.

Table 4
Summary of Open Circuit Potential (mV_{SCE}) Data

Simulant	Bullet		Mill-Scale		Partial Mill-Scale	
	Initial	After	Initial	After	Initial	After
AY-101	-557	-140	-175	-140	-388	-140
SY-101	-492	-74	-183	-298	-324	-340
AW-105 with small organic acids (i.e., formate, acetate, glycolate)	-668	-256	-284	-186	-405	-319
AW-105 with small organic acids plus tributylphosphate family plus normal paraffin hydrocarbon	-516	-239	-205	-237	–	–
AW-105 with small organic acids plus spiked tributylphosphate family plus normal paraffin hydrocarbon	-893	-494	-300	-459	-299	-480

Table 5
Open Circuit Potential (mV_{SCE}) Data of Tanks

Tank	Years of Service	Initial Potential (mV_{SCE})	Final Potential (mV_{SCE})	Average Potential (mV_{SCE})	Std. Dev. (mV_{SCE})
AY-101	0.5	-80	-74	-77	NA
SY-101	5.5	-257	-279	-257	13
AW-105	6.5	-253	-394	-345	78

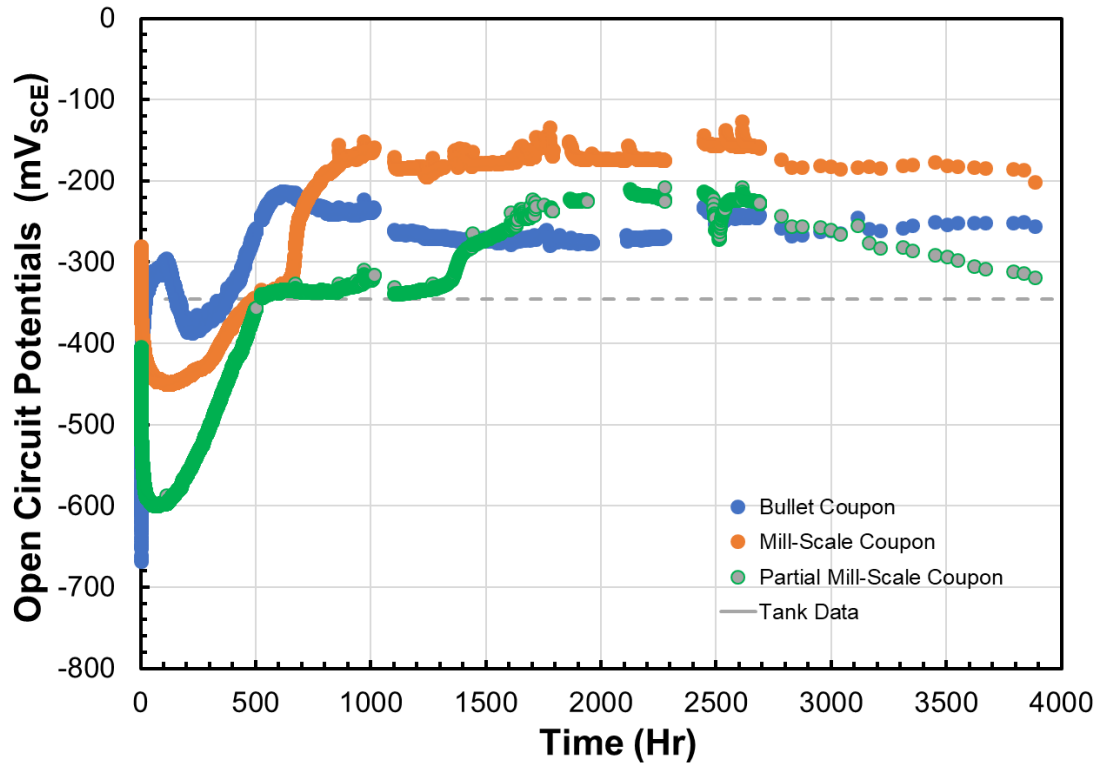

Figure 4: Open Circuit Potential data for the bullet (600-grit polished surface), mill-scale, and partial mill-scale coupons in AW-105 simulant containing small organic acids

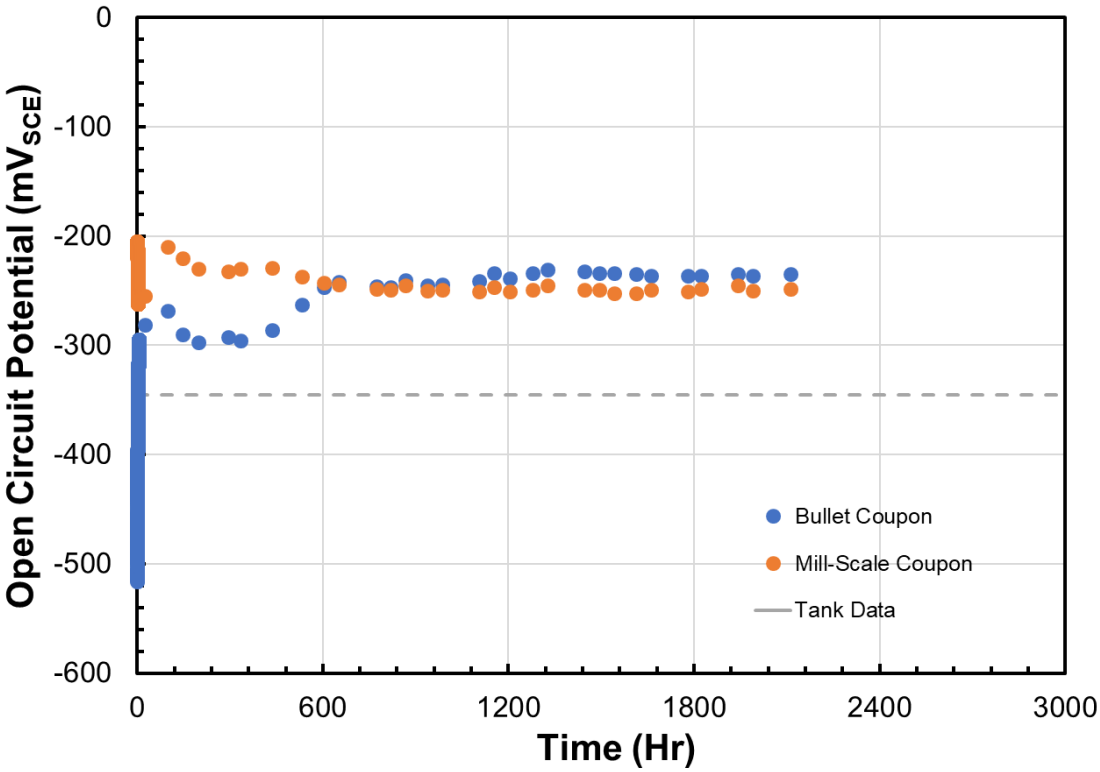

Figure 5: Open Circuit Potential data for the bullet (600-grit polished surface) and mill-scale coupons in AW-105 simulant small organic acids plus tributylphosphate family plus normal paraffin hydrocarbon

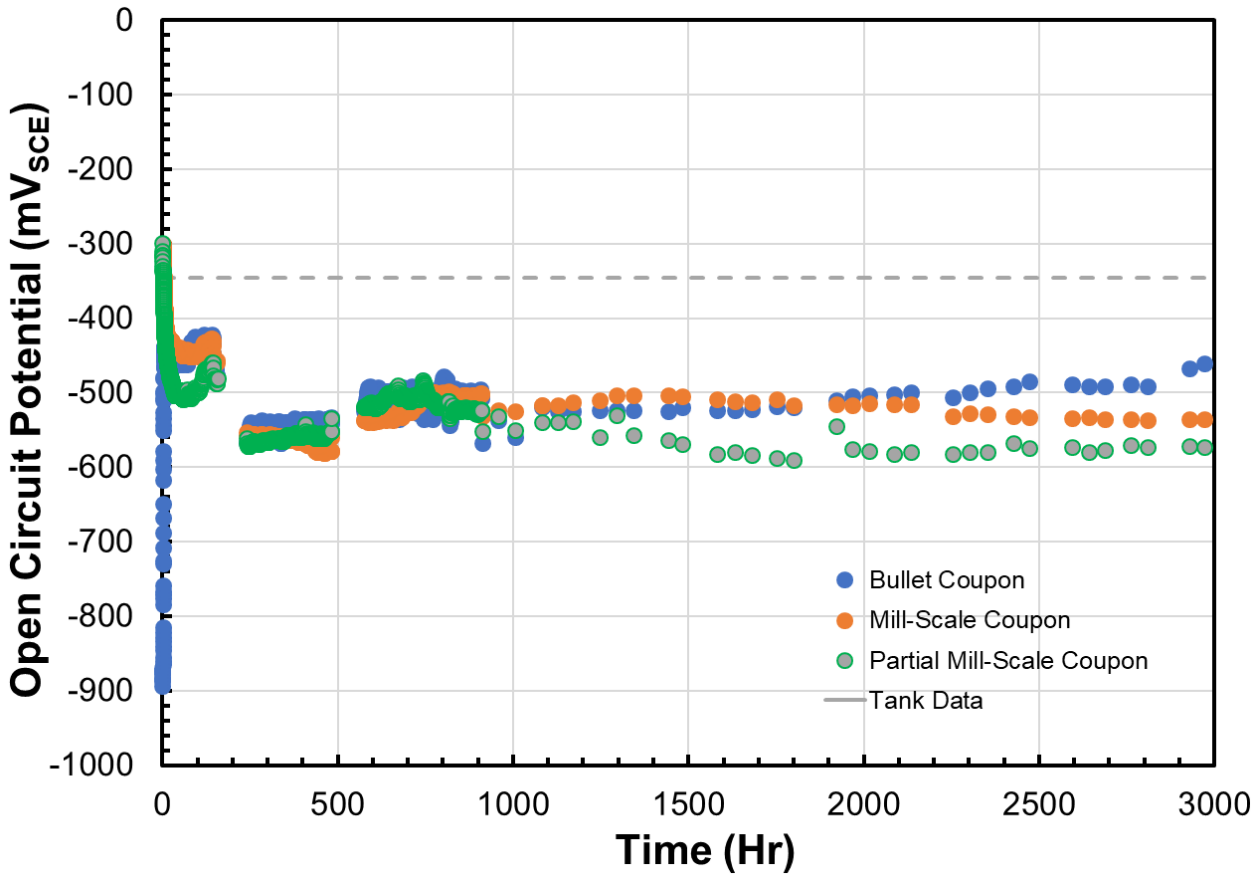

Figure 6: Open Circuit Potential data for the bullet (600-grit polished surface), mill-scale, and partial mill-scale coupons in AW-105 simulant containing small organic acids plus spiked tributylphosphate family plus normal paraffin hydrocarbon

The tank data listed in Table 5 is compared with AY-101 and SY-101 simulant data. For AY-101 simulant, the OCPs are -140 mV_{SCE} for all three coupons whereas the tank wall OCP was measured to be -79 mV_{SCE}. Thus, the tank wall OCP is 60 mV more anodic than the simulant OCP. SY-101 simulant OCPs are different for each electrode: -73 mV_{SCE} , -298 mV_{SCE} , and -340 mV_{SCE} for the bullet, mill-scale, and partial mill-scale coupons; the tank wall OCP was measured to be -257 ± 13 mV_{SCE}. The tank-wall OCP is closest to the mill-scale coupon.

The tank data for AW-105, listed in Table 5, are compared with the AW-105 simulant data. The tank-wall potential was measured to be -345 ± 78 mV_{SCE}. The OCPs of the electrode after 4000 hours in AW-105 with small organic acids are following: -201 mV_{SCE}, -256 mV_{SCE} , , and -319 mV_{SCE} for the bullet, mill-scale, and partial mill-scale coupons; this indicate that he partial-mill scale coupon's OCP is within the range of the tank data. Similarly, the OCPs of the electrode after 2100 hours in AW-105 with small organic acids plus tributylphosphate family plus normal paraffin hydrocarbon are following: -239 mV_{SCE} and -251 mV_{SCE} for the bullet and mill-scale coupons, respectively; these OCPs are similar to the bullet coupon OCP in AW-105 with small organic acids, but do not fall in the range of -345 ± 78 mV_{SCE}, i.e., -267 to -423 mV_{SCE}. The OCPs of the coupons in AW-105 simulant containing small organic acids plus spiked tributylphosphate family plus normal paraffin hydrocarbons after 4000 hours are following: -461 mV_{SCE} , -535 mV_{SCE} , and -573 mV_{SCE} for the bullet, mill-scale, and partial mill-scale coupons; none of the three coupons' OCP fall in the tank-wall OCP. The comparison between the simulants' and tank data is summarized in Table 6.

Table 6
Comparison of Tank Wall and Simulant Open Circuit Potential Data

Tank	Tank-Wall Open Circuit Potential	Simulant Open Circuit Potential Data and Notes
AY-101	-77 mV_{SCE}	• -140 mV_{SCE} for all three coupons; simulant OCPs are -63 mV more cathodic than the tank-wall OCP
SY-101	-257 ± 13 mV_{SCE} (-244 to -270 mV_{SCE})	• -73 mV_{SCE} , -298 mV_{SCE} , and -340 mV_{SCE} for the bullet, mill-scale, and partial mill-scale coupons, respectively • Mill-scale coupon's OCP are closest to the tank-wall data
AW-105	-345 ± 78 mV_{SCE} (-267 to -423 mV_{SCE})	AW-105 with small organic acids • -201 mV_{SCE}, -256 mV_{SCE}, and -319 mV_{SCE} for the bullet, mill-scale, and partial mill-scale coupons, respectively • Partial mill-scale coupon's OCP is within the tank-wall OCP range • Mill-scale and bullet coupons' OCPs are close to the tank data
		AW-105 with small organic acids plus tributylphosphate family plus normal paraffin hydrocarbon • -239 mV_{SCE} and -251 mV_{SCE} for the bullet and mill-scale coupons, respectively • Both bullet and mill-scale coupons' OCPs are near the range, within 30 mV of the tank data
		AW-105 with small organic acids plus spiked tributylphosphate family plus normal paraffin hydrocarbon • -461 mV_{SCE} , -535 mV_{SCE} , and -573 mV_{SCE} for the bullet, mill-scale, and partial mill-scale coupons, respectively • Coupons' OCPs are outside the range

The CPP data were collected for AY-101, SY-101, and AW-105 with small organic acid simulants; the data were collected after OCP hold and EIS measurements and are presented in Figure 7, and coupons' images are presented in Figure 8.

The CPP data for the bullet, mill-scale, and partial mill-scale coupons in AY-101 simulant is presented in Figure 7(a). The three coupons' CPP responses exhibit negative hysteresis, i.e., pitting corrosion of the electrode material is unlikely in the simulant chemistry. The passive current density of the bullet coupon is approximately 2×10^{-4} mA/cm^2. It is noted that the passive current density of the bullet coupon is about two orders of magnitude lower than the mill-scale and partial-mill coupons. There are two plausible explanation for the higher passive current densities of the mill-scale and partial mill-scale coupons: (i) there are anodic reactions other than the metal dissolution reactions that occur on the mill-scale and partial mill-scale coupons leading to higher current densities during the forward scans of the CPP curves, and (ii) the passive film that develops on the polished surface could not be fully developed due to presence of mill-scale and corrosion products on the mill-scale and partial mill-scale coupons. These two hypotheses require further investigations.

The CPP data for the bullet, mill-scale, and partial mill-scale coupons in SY-101 simulant is presented in Figure 7(b). The three coupons' CPP responses exhibit negative hysteresis, i.e., pitting corrosion of the electrode material is unlikely in the simulant chemistry. The passive current density of the bullet coupon is approximately 4×10^{-4} mA/cm^2. Compared to the mill-scale and partial mill-scale coupons, the passive current density of the bullet coupon is about two orders of magnitude lower. As mentioned previously, the two plausible explanations could be due to anodic reactions other than the metal dissolution on the mill-scale and corrosion product layer of the mill-scale and partial mill-scale coupons, and lack of complete passive film on the mill-scale and partial mill-scale coupons.

The CPP data for the bullet, mill-scale, and partial mill-scale coupons in AW-105 simulant with small organic acids is presented in Figure 7(c). The three coupons' CPP responses exhibit negative hysteresis, i.e., pitting corrosion of the electrode material is unlikely in the simulant chemistry. The passive current density of the bullet coupon is in the range of 10^{-4} to 10^{-3} mA/cm^2. Compared to the mill-scale and partial mill-scale coupons, the passive current density of the bullet coupon is about one-two orders of magnitude lower. The two plausible explanations,

as mentioned previously, could be the cause of higher passive current density in the mill-scale and partial mill-scale coupons compared to the bullet coupon.

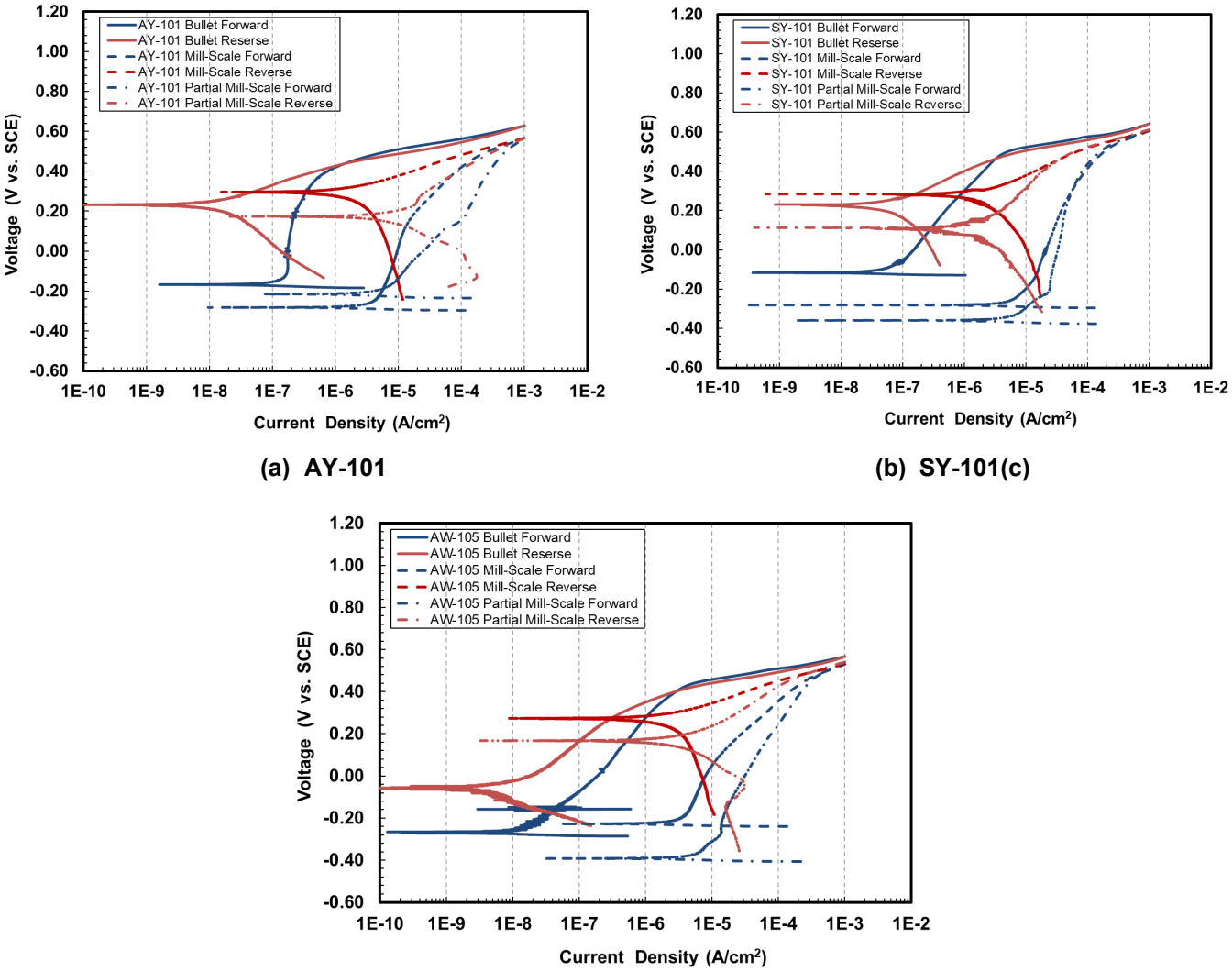

Figure 7: CPP data for the bullet, mill-scale, and partial mill-scale coupons after OCP holds in AY-101, SY-101 and AW-105 with small organic acids

Images of the coupons after OCP hold, EIS and CPP measurements are presented in Figure 8. Images of the bullet, mill-scale, and partial mill-scale coupons in AY-101 simulant are presented in Figures 8(a), 8(b), and 8(c), respectively. Although discoloration of the coupons did occur, no visible signs of pitting corrosion were observed on the three coupons. Similarly, images of the bullet, mill-scale, and partial mill-scale coupons in SY-101 simulant are presented in Figures 8(d), 8(e), and 8(f), respectively. No visible signs of the pitting corrosions were observed in the three coupons in SY-101 simulant. In addition, discoloration of the coupons in SY-101 was not as severe as in AY-101 simulant. Images of the bullet, mill-scale, and partial mill-scale coupons in AW-105 simulant with small organic acids are presented in Figures 8(g), 8(h), and 8(i), respectively. Similar to AY-101 and SY-101, coupons discoloration did occur in the AW-105 simulant, but no visible signs of pitting corrosion were observed in the three coupons.

EIS data for the coupons in AY-101, SY-101, and AW-105 with small organic acids are presented in Figure 9. EIS measurements were conducted in the frequency range of 10^4 to 10^{-4} Hz. EIS data for the bullet, mill-scale, and partial mill-scale coupons in AY-101 simulant are presented Figures 9(a). Similarly, EIS data for the coupons in SY-101 and AW-105 simulants are presented in Figures 9(b) and 9(c), respectively. The following observations were made for the impedance spectra of the coupons:

- Even at the low-end frequency spectra of the both sets of coupons, the asymptotic impedance values could not be measured, indicating that charge transfer resistances associated with the metal interface reactions are higher than the lowest frequency impedance values.

- All impedance data exhibit a single time-constant type response, indicating that activation-control reaction kinetics is dominant for the three electrode.

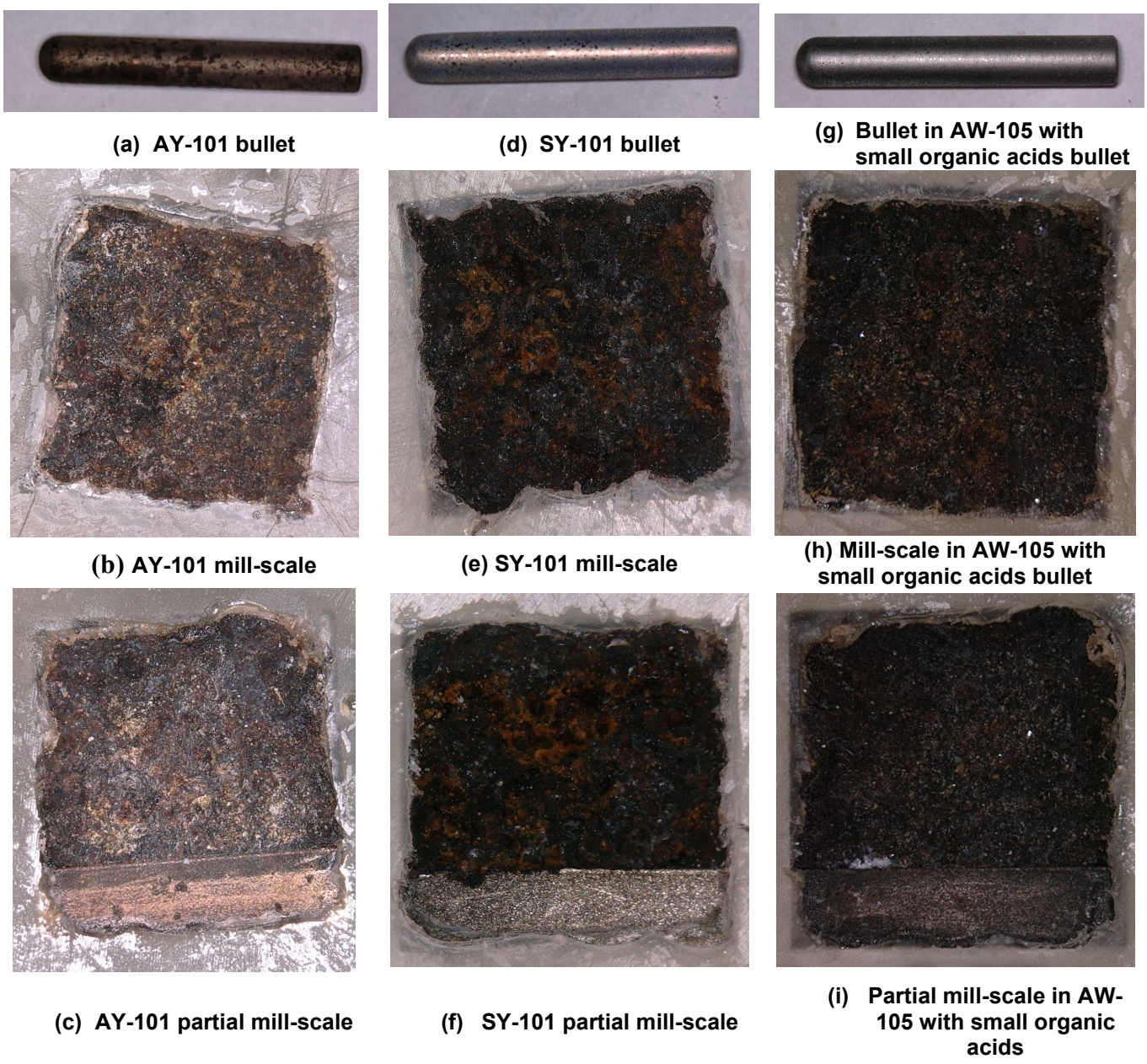

(a) AY-101 bullet **(d) SY-101 bullet** **(g) Bullet in AW-105 with small organic acids bullet**

(b) AY-101 mill-scale **(e) SY-101 mill-scale** **(h) Mill-scale in AW-105 with small organic acids bullet**

(c) AY-101 partial mill-scale **(f) SY-101 partial mill-scale** **(i) Partial mill-scale in AW-105 with small organic acids**

Figure 9: Images of the bullet, mill-scale, and partial mill-scale coupons in AY-101, SY-101, and AW-105 with small organic after OCP holds, CPP, and EIS measurements

- Low frequency impedances of the mill-scale and partial mill-scale coupons are lower than bullet coupon impedance in AY-101, SY-101, and AW-105 with small organic acids. This indicates that polarization resistance of the bullet coupons in the three simulants is higher than the mill-scale and partial mill-scale coupons. This observation is also consistent with the CPP data where higher passive current densities were observed for the mill-scale and partial mill-scale coupons compared to the bullet coupons in the three simulants.

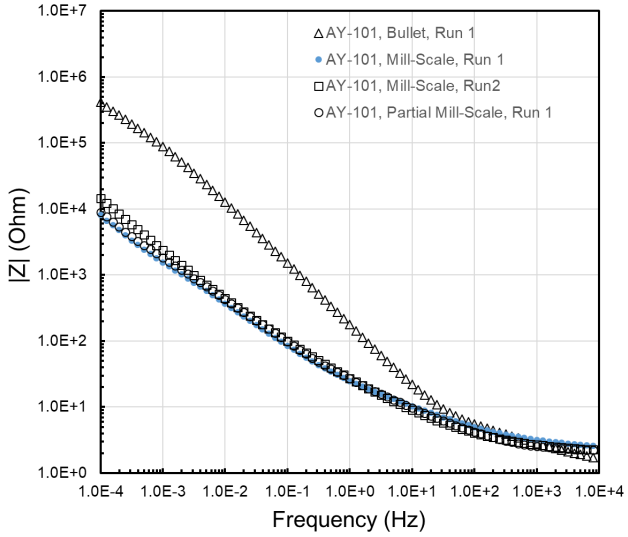

(a) AY-101

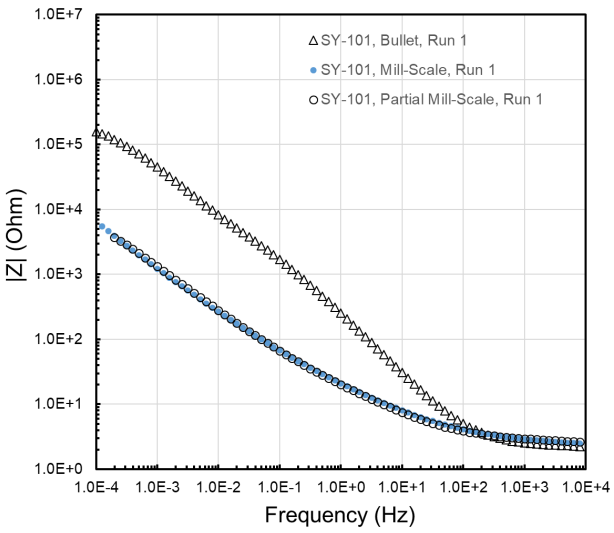

(b) SY-101

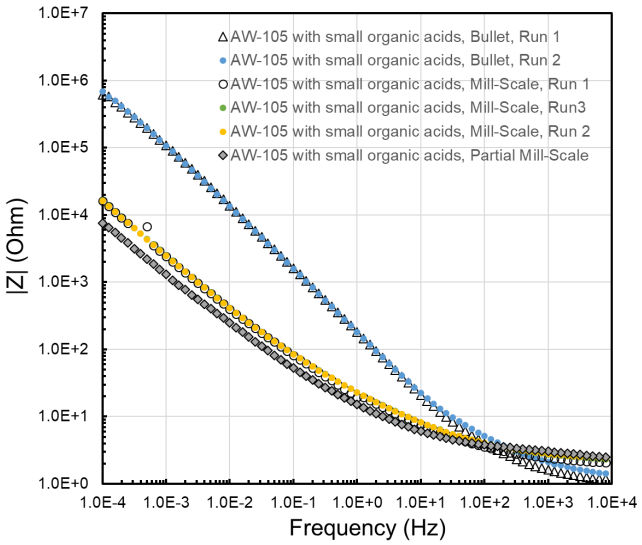

(c) AW-105 with small organic acid

Figure 9: EIS data for bullet, mill-scale, and partial mill-scale coupons in AY-101, SY-101, and AW-105 with small organic acid simulants

These studies also highlight effects of open circuit potential evolutions on stress corrosion cracking. An example of this is AY-101 where tank potential is -70 mV_{SCE}, but the long-term laboratory data indicate the potential of approximately -140 mV_{SCE}. Stress corrosion cracking experimental studies with a simulated related to AY-101 30°C did not exhibit SCC at OCP + 100 mV_{SCE}, OCP + 200 mV_{SCE}, or OCP + 300 mV_{SCE}, however OCP values for the similar chemistry were -300, -360 to -287 mV_{SCE}. This indicate that though the SCC risk is certainly small because the AY-101 waste is stored at relatively low temperature, the reported OCP values are far different from the other laboratory measurements.

CONCLUSION

Corrosion potential is one of the key parameters in determining pitting corrosion and stress corrosion cracking propensity of the Hanford's double shell tank carbon steel. Evolution of corrosion potentials was studies for three tank waste simulants identified as AY-101, SY-101, and AW-105. Coupons with three different surface conditions were placed in each tank chemistry. The surface conditions included polished, mill-scale, and partial mill-scale. The corrosion potentials of the coupons with the three different conditions evolved to same value in AY-101 simulant, and appeared to reach a steady state. The coupons' corrosion potentials in SY-101 differed as much as

by 250 mV, and continued to evolve even after 4000 hours of exposure. The corrosion potentials of the coupons in AW-105 with small organic acids were in the range of -200 to -300 mV_{SCE} after 4000 hours of exposure. Similarly, corrosion potentials of the coupons in AW-105 with small organic acids plus tributylphosphate family plus normal paraffin hydrocarbon were also in -200 to -300 mV_{SCE} after 2100 hours of exposure. The corrosion potentials of the coupons in AW-105 with small organic acids plus spiked tributylphosphate family plus normal paraffin hydrocarbon were in the range of -450 to -600 mV_{SCE} after 4000 hours of exposure. The CPP data for the three coupon types in the three simulants exhibited category one response, i.e., pitting corrosion of the tank steel is unlikely in the three simulants. However passive current density of the mill-scale and partial mill-scale coupons was one-two orders of magnitude higher than the bullet coupons in all three simulant chemistries; similar trends were observed in the EIS data of the three coupon types in the three simulants. The low frequency impedance of the mill-scale and partial mill-scale coupons were lower than the bullet coupons impedance. The EIS and CPP data are cross-consistent, i.e., evidence of bullet coupons' lower passive current density compared to mill-scale and partial mill-scale coupons in the CPP current is exhibited in form of higher impedances of the bullet coupons compared to the other two coupon types. There are two plausible explanation for the higher passive current densities of the mill-scale and partial mill-scale coupons compared to the bullet coupons: (i) there are anodic reactions other than the metal dissolution reactions that occur on the mill-scale and partial mill-scale coupons leading to higher current densities during the forward scans of the CPP curves, and (ii) the passive film that develops on the polished surface could not be fully developed due to presence of mill-scale and corrosion products on the mill-scale and partial mill-scale coupons. These two hypotheses require further investigations.

REFERENCES

1. P. K. Shukla "Chapter 7 – Thermodynamics of corrosion and potentiometric methods for measuring localized corrosion," In Techniques for Corrosion Monitoring, Ed. L.Yang, Woodhead Publishing Limited, pp. 156-186. 2008.

2. S. Chawla, K. Evans, K.M. Sherer, J. A. Beavers, and N. Sridhar, "Electrochemical Studies of Open-Circuit Potential Drift of Carbon Steel in Nuclear Waste Simulants," CORROSION/2017, paper no. C2017-9789 (Houston, TX, NACE, 2017).

3. K. Evans, S. Chawla, K.M. Sherer, K.D. Boomer, "The Passive Film Evolution of Carbon Steel in Hanford Waste Simulants," CORROSION/2018, paper no. C2018-11016 (Houston, TX, NACE, 2018).

4. ASTM International. ASTM G61 - 86(reapproved 2018), "Standard Test Method for Conducting Cyclic Potentiodynamic Polarization Measurements for Localized Corrosion Susceptibility of Iron-, Nickel-, or Cobalt-Based Alloys." West Conshohocken, Pennsylvania: ASTM International. 2018.

5. R. E. Fuentes, B. J. Wiersma, K. D. Boomer and A. J. Feero, "Inhibition of Pitting Corrosion in Simulated Liquid Radioactive Waste", CORROSION/2017, Paper No. 9689 (Houston, TX, NACE, 2017).

6. R. E. Fuentes, B. J. Wiersma, K. D. Boomer and A. J. Kim, "Pitting Corrosion Inhibition of Carbon Steel in Simulated Liquid Radioactive Waste at Elevated Hydroxide Concentrations", CORROSION/2018, Paper No. 51318-11456 (Houston, TX, NACE, 2018).